Energy Conversion

DOI: 10.1002/ange.201406982

Platinum-Free Binary Co-Ni Alloy Counter Electrodes for Efficient Dye-Sensitized Solar Cells**

Xiaoxu Chen, Qunwei Tang, Benlin He, Lin Lin, and Liangmin Yu**

Abstract: *Dye-sensitized solar cells (DSSCs) have attracted growing interest because of their application in renewable energy technologies in developing modern low-carbon economies. However, the commercial application of DSSCs has been hindered by the high expenses of platinum (Pt) counter electrodes (CEs). Here we use Pt-free binary Co-Ni alloys synthesized by a mild hydrothermal strategy as CE materials in efficient DSSCs. As a result of the rapid charge transfer, good electrical conduction, and reasonable electrocatalysis, the power conversion efficiencies of Co-Ni-based DSSCs are higher than those of Pt-only CEs, and the fabrication expense is markedly reduced. The DSSCs based on a $CoNi_{0.25}$ alloy CE displays an impressive power conversion efficiency of 8.39 %, fast start-up, multiple start/stop cycling, and good stability under extended irradiation.*

Dye-sensitized solar cells (DSSCs),[1–3] electrochemical devices that convert solar energy into electricity, are considered to be one of the promising solutions to energy depletion, environmental pollution, and ecological destruction because of their easy fabrication, cost-effectiveness, and relatively high power conversion efficiency. Although the first prototype was described in 1991 by O′Regan and Grätzel,[1] DSSCs have not yet been commercialized, but great achievements have been made. One of the main problems is the high expense of the platinum counter electrode (Pt CE), an electrocatalyst for reducing triiodides (I_3^-) to iodides (I^-). Pt-free CEs based on carbon and conductive polymer materials have been developed to overcome this problem.[4–7] The overall power conversion efficiencies of DSSCs with these Pt-free CEs are generally lower than 7.5 %,[8,9] which is similar to that of Pt-based DSSCs. However, such Pt-free CEs have a common drawback in terms of their long-term operation because of their unsatisfactory charge-transfer ability.[10,11] One promising solution is the alloying of transition metals with other metals or nonmetals to generate cost-effective CEs. Wang and co-workers reported the utilization of metal selenide CEs in DSSCs,[10] with the $Co_{0.85}Se$ and $Ni_{0.85}Se$ CEs synthesized by a hydrothermal approach. The proposed metal selenides exhibited much higher electrocatalytic activity than Pt for I_3^- reduction, and generated a promising efficiency of 9.40 % in their DSSC device. More recently, an alloy CE from the $CuInGaSe_2$ alloy was prepared by a magnetron sputtering technology, which gave a conversion efficiency of 7.13 % in its DSSC.[12] Moreover, a binary Au-Ag alloy was also employed as a CE material in DSSC, and demonstrated an efficiency of 7.85 %.[13] The recent results from our research group indicated that binary Co-Pt alloy CEs are more efficient than Pt-Ru electrodes.[14–16] A promising power conversion efficiency of 10.23 % was determined using an electrochemically co-deposited $CoPt_{0.02}$ alloy CE.[14] Although the research on alloy CEs is still preliminary, the impressive merits along with scalable components demonstrate them to be good candidates in robust DSSCs.

To explore other efficient Pt-free CEs, we synthesized a new type of binary Co-Ni alloy CE for DSSC application by a mild hydrothermal reduction strategy. The resultant Co-Ni alloy CEs display intrinsic electrocatalytic activity toward the reduction of I_3^- ions, a rapid charge-transfer ability, and cost-effectiveness. These merits demonstrate the Co-Ni alloys to be potential electrocatalysts in robust DSSCs. A DSSC with a $CoNi_{0.25}$ alloy CE shows a power conversion efficiency as high as 8.39 %, which is much higher than the 6.96 % from expensive Pt-based DSSCs.

The binary Co-Ni alloy CEs synthesized by a mild hydrothermal reduction method were subjected to X-ray diffraction (XRD) measurements. The XRD results indicate that the as-prepared CEs consist of Co-Ni alloys with a face-centered cubic (fcc) structure and FTO glass substrates (Figure 1).[17] Scanning electron microscopy (SEM) photographs (Figure 2 a–e) suggest a high surface coverage of the Co-Ni alloy on the FTO substrate. Close examination shows homogeneous spherical aggregations of approximately 200 nm diameter. The loose structure of the Co-Ni alloys at Ni dosages lower than 0.33 provides facile channels for the transportation of I^-/I_3^- species. Lattice fringes are clearly observed in the HRTEM image of the $CoNi_{0.25}$ alloy (Figure 2 f), which indicates the resultant alloy has high crystallinity. The measured spacing between the crystallographic

[*] X. Chen, Prof. Q. Tang, Dr. B. He, Prof. L. Yu
Key Laboratory of Marine Chemistry Theory and Technology
Ministry of Education, Ocean University of China
Institute of Materials Science and Engineering
Ocean University of China
238 Songling Road, Laoshan District, Qingdao 266100 (P.R. China)
E-mail: tangqunwei@ouc.edu.cn
yuyan@ouc.edu.cn
Dr. L. Lin
National Engineering Research Center for Nanotechnology
Shanghai 200241 (P.R. China)

[**] We would like to acknowledge financial support from the Fundamental Research Funds for the Central Universities (201313001, 201312005), Shandong Province Outstanding Youth Scientist Foundation Plan (BS2013CL015), Shandong Provincial Natural Science Foundation (ZR2011BQ017), Research Project for the Application Foundation in Qingdao (13–4–198-jch), National Key Technology Support Program (2012BAB15B02), and National High-Tech Research and Development Programme of China (2010AA09Z203, 2010AA065104).

Supporting information for this article is available on the WWW under http://dx.doi.org/10.1002/anie.201406982.

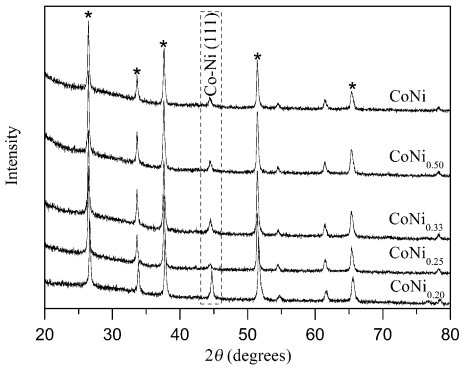

Figure 1. XRD patterns of binary Co-Ni alloy CEs. The diffraction peaks labeled with (*) were attributed to fluorine-doped tin oxide (FTO) conductive glass.

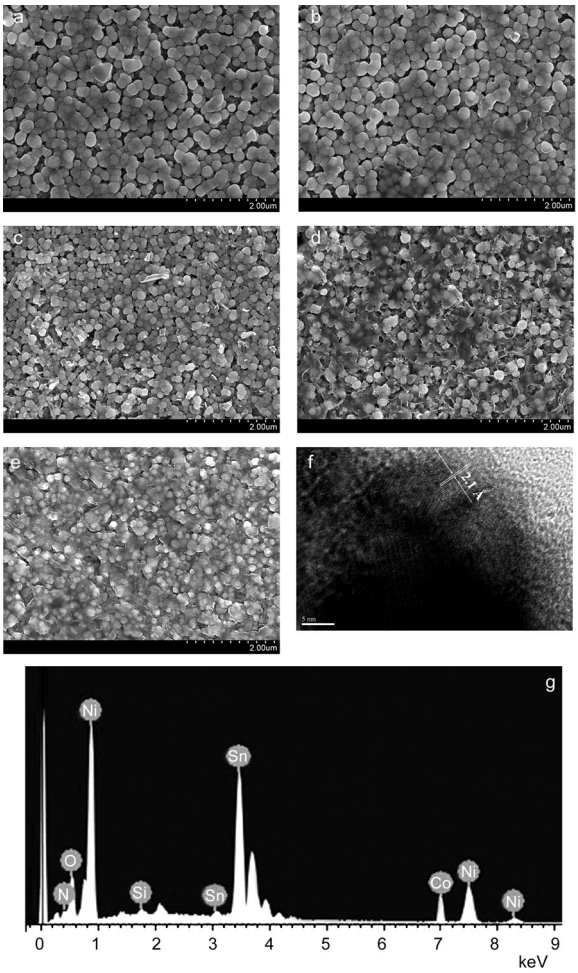

Figure 2. SEM photographs of a) $CoNi_{0.20}$, b) $CoNi_{0.25}$, c) $CoNi_{0.33}$, d) $CoNi_{0.50}$, and e) CoNi alloys supported on a FTO substrate. f) HRTEM image and g) EDX spectrum of a $CoNi_{0.25}$ alloy CE.

planes is 2.1 Å for the (111) plane. Moreover, many lattice distortions ($\Delta d/d$) are evident in the crystal lattices. $\Delta d/d$ can be obtained from $\Delta d/d = \beta/4\,tg\theta$,[18] where β is the line width at half-maximum height, and θ is the diffraction angle. The order of the calculated $\Delta d/d$ values is: $CoNi_{0.25}$ (0.0091) > $CoNi_{0.33}$ (0.0073) > $CoNi_{0.50}$ (0.0072) > $CoNi_{0.20}$ (0.0059) > CoNi (0.0033). These results demonstrate that the alloying of Co and Ni can form defects, which provide large active sites for I_3^- adsorption and reduction. Co and Ni as well as the elements from the FTO substrate are evident in the energy-dispersive X-ray (EDX) spectrum (Figure 2g), which indicates that Co and Ni have been successfully deposited on the FTO glass substrate. The atomic ratios of the Co-Ni alloys were determined by ICP-AES to be 1.000:0.218 for $CoNi_{0.20}$, 1.000:0.241 for $CoNi_{0.25}$, 1.000:0.337 for $CoNi_{0.33}$, 1.000:0.488 for $CoNi_{0.50}$, and 1.000:1.013 for CoNi. The recorded atomic ratios are similar to the stoichiometry, therefore, the chemical formulas of the binary Co-Ni alloys can be expressed according to their stoichiometric ratios.[10]

XPS analysis was carried out to characterize the chemical structure and composition of the resultant $CoNi_{0.25}$ alloy. The peaks for $Co2p_{3/2}$ and $Ni2p_{3/2}$ are centered at 778.32 and 853.12 eV, respectively, in the case of pure $CoNi_{0.25}$ alloys (see Figure S1 in the Supporting Information). These binding energies are attributed to the features of the Co-Ni alloy phase.[19] Moreover, the peaks corresponding to O1s and metal oxides or hydroxides are not observed in the resultant alloy, thus confirming the metallic nature of the as-prepared $CoNi_{0.25}$ alloy. This conclusion is consistent with the composition analysis. It has been noted that the alloying of transition metals can favor the electronic perturbation of the other metals,[20,21] and, therefore, accelerate the electrocatalytic activity of the alloys.

Figure 3a shows the characteristic *J-V* curves of the DSSCs based on Co-Ni alloys, Pt, Co, and Ni as the CEs. The detailed photovoltaic parameters from the *J-V* curves are summarized in Table 1. The DSSC with a $CoNi_{0.25}$ CE yields a remarkable $\eta = 8.39\,\%$, $J_{sc} = 18.02\ mA\,cm^{-2}$, $V_{oc} = 0.706$ V, and $FF = 0.66$, which are much higher than the photovoltaic

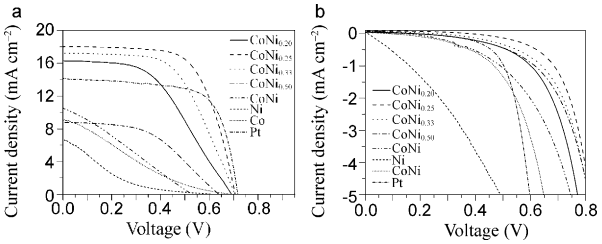

Figure 3. Characteristic *J-V* curves of DSSCs with various CEs: a) under one sun illumination and b) in the dark.

Table 1: Photovoltaic parameters of DSSCs with varied CEs and the simulated data from EIS spectra.[a]

CEs	η [%]	V_{oc} [V]	*FF*	J_{sc} [mA cm^{-2}]	R_{ct} [Ω cm^2]
CoNi	1.51	0.530	0.27	10.49	126.5
$CoNi_{0.50}$	2.69	0.639	0.48	8.72	33.9
$CoNi_{0.33}$	6.93	0.705	0.57	17.25	32.3
$CoNi_{0.25}$	8.39	0.706	0.66	18.02	27.2
$CoNi_{0.20}$	5.37	0.691	0.48	16.30	64.5
Pt	6.96	0.715	0.69	14.17	33.9
Co	1.27	0.675	0.21	9.14	301.6
Ni	0.54	0.616	0.13	6.62	346.7

[a] V_{oc}: open-circuit voltage; J_{sc}: short-circuit current density, *FF*: fill factor; η: power conversion efficiency; R_{ct}: charge-transfer resistance.

parameters obtained with pure Pt, Co, or Ni. It is noteworthy that the V_{oc}, J_{sc}, and *FF* values for a DSSC based on a $CoNi_{0.25}$ CE are also higher than those of the DSSC devices with other alloys. This may be attributed to the fact that the rapid interconversion between I_3^- and I^- (see Figure S2 in the Supporting Information) can accelerate the generation of photoelectrons from dye molecules and, therefore, elevate the electron flow from the excited dye to the conduction band of the TiO_2 and so lead to accumulation of electron density in the conduction band of TiO_2.[22] The recorded efficiency from the $CoNi_{0.25}$ alloy CE is impressive for DSSCs with Pt-free catalysts.

An electrochemical impedance spectroscopy (EIS) experiment was carried out on a symmetric dummy cell fabricated with two identical CEs to confirm the catalytic activities of the alloys and pure Co or pure Ni; the R_{ct} values are also summarized in Table 1. The Nyquist plots (Figure 4a)

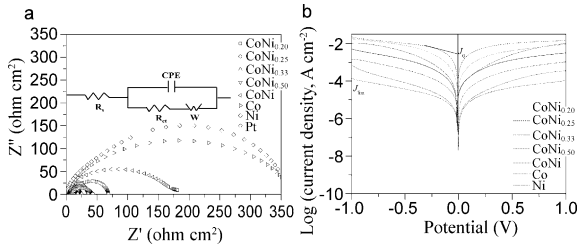

Figure 4. a) Nyquist plots and b) Tafel polarization curves for symmetric dummy cells fabricated with two identical CEs. The inset shows the equivalent circuit.

illustrate that the $CoNi_{0.25}$ CE has $R_{ct} = 27.2\ \Omega\,cm^2$, which is smaller than the others. This result indicates that the formation of the Co-Ni alloy from Co and Ni has an accelerating effect on the charge-transfer ability. The rapid reduction of I_3^- to I^- is expected to enhance dye recovery and electron generation. Therefore, photogenerated electrons can easily flow to the conduction band of TiO_2 under an increased potential drop, thus ultimately giving an enhanced J_{sc} value. Moreover, the optimal *FF* value is also easily determined in a DSSC with a $CoNi_{0.25}$ CE because of the dependence of *FF* on R_{ct}.[23]

Figure 4b displays the Tafel polarization curves measured on the symmetrical dummy cells used in the EIS experiments. The slopes of the anodic or cathodic branches are in the order: $CoNi_{0.25} > CoNi_{0.33} > CoNi_{0.50} > CoNi_{0.20} > CoNi > Co > Ni$. A larger slope in the anode or cathodic branch indicates a higher exchange current density (J_0) on the CE, as a result of a high alloy loading and a porous structure. The J_0 value can be calculated from $J_0 = RT/nFR_{ct}$,[24] where R is the gas constant, T is the absolute temperature, F is Faraday's constant, and R_{ct} is charge-transfer resistance obtained from the EIS plots. The order of the calculated R_{ct} values is $CoNi_{0.25} < CoNi_{0.33} < CoNi_{0.50} < CoNi_{0.20} < CoNi < Co < Ni$, which is consistent with the result from the EIS analysis. Additionally, the intersection of the cathodic branch with the *y*-axis can be considered as the limiting diffusion current density (J_{lim}), a parameter that depends on the diffusion coefficient of I^-/I_3^- redox couples in an electrolyte because of a diffusion-controlled mechanism (see Figure S2b in the Supporting Information). The diffusion coefficient (D_n) of the redox species is proportional to J_{lim}[25] through $D_n = lJ_{lim}/2nFC$, where l is the spacer thickness, and C is the concentration of I_3^- ions. From Figure 4b, one can find that both the J_{lim} and D_n values follow the order of $CoNi_{0.25}$ ($5.30 \times 10^{-8}\ cm^{-2}\,s^{-1}$) > $CoNi_{0.33}$ ($2.92 \times 10^{-8}\ cm^{-2}\,s^{-1}$) > $CoNi_{0.50}$ ($2.85 \times 10^{-8}\ cm^{-2}\,s^{-1}$) > $CoNi_{0.20}$ ($1.34 \times 10^{-8}\ cm^{-2}\,s^{-1}$) > CoNi ($1.29 \times 10^{-8}\ cm^{-2}\,s^{-1}$) > Co ($3.46 \times 10^{-10}\ cm^{-2}\,s^{-1}$) > Ni ($1.17 \times 10^{-10}\ cm^{-2}\,s^{-1}$). Alternatively, the D_n value can also be described by Randles–Sevcik theory:[26] $J_{red} = Kn^{1.5}ACD_n^{0.5}v^{0.5}$, where J_{red} is the peak current density for $I_3^- + 2e \rightarrow 3I_3^-$, K is 2.69×10^5, n is the number of electrons participating in the reduction reaction, A is the electron area, C represents the bulk concentration of I_3^-, and v is the scan rate for the cyclic voltammetry (CV) curves. The D_n value obtained by CV measurement is in a good agreement with that from Tafel analysis (see Figure S2a in the Supporting Information).

Figure 5a represents the Bode spectra of symmetric dummy cells from various CEs. The liftetimes of electrons parcitipating in the I_3^- reduction reaction (τ_1) can be represented as $\tau_1 = 1/2\pi f_p$,[27] where f_p is the peak frequency in the Bode spectra. The order of the calculated τ_1 values for I_3^- reduction (Table 2) is 77.7 μs ($CoNi_{0.25}$) < 89.5 μs ($CoNi_{0.33}$) < 178.1 μs ($CoNi_{0.50}$) < 195.7 μs ($CoNi_{0.20}$) < 313.6 μs (CoNi) < 636.2 μs (Co) < 1317.1 μs (Ni). Considering that the task of a CE is to collect electrons from an external circuit and to reduce I_3^- to I^- ions, τ_1, therefore, implies the required time for the I_3^- reduction reaction by the CE. The electrons within the $CoNi_{0.25}$ alloy CE apparently have the shortest lifetime, which suggests that the $CoNi_{0.25}$ CE has the highest electrocatalytic activity toward I_3^- reduction. The conclusions for the electrocatalytic activity derived from the EIS and CV data are consistent. However, the parameter τ_2 in DSSC devices indicates the lifetime of electrons in the TiO_2 photoanode (Figure 5b). A larger τ_2 value within TiO_2

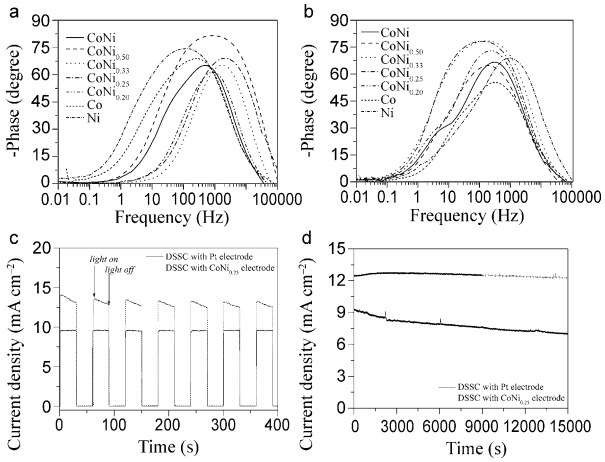

Figure 5. Bode phase plots of a) symmetric dummy cells and b) DSSCs with various CEs. c) Start-stop switches and d) photocurrent stabilities of the DSSCs with $CoNi_{0.25}$ alloy and Pt electrodes. The on-off plots were achieved by alternately irradiating (100 mW cm^{-2}) and darkening (0 mW cm^{-2}) the DSSC devices at 0 V, whereas the photocurrent stabilities were carried out under a sustained irradiation of 100 mW cm^{-2}.

Table 2: Lifetimes of the electrons in the I_3^- reduction reaction and transportation in the TiO_2 photoanode.[b]

CEs	Frequency$_1$ [Hz]	τ_1 [μs]	Frequency$_2$ [Hz]	τ_2 [μs]
CoNi	507.8	313.6	314.3	506.6
$CoNi_{0.50}$	894.3	178.1	191.9	829.8
$CoNi_{0.33}$	1778.3	89.5	158.7	1003.4
$CoNi_{0.25}$	2048.6	77.7	131.3	1212.8
$CoNi_{0.20}$	813.8	195.7	249.0	639.5
Co	250.3	636.2	315.7	504.4
Ni	120.9	1317.1	1033.5	154.1

[b] Frequency$_1$: the peak frequencies for the symmetric dummy cells; τ_1: lifetime of the electrons in the I_3^- reduction reaction; Frequency$_2$: the second peak frequency for the DSSCs; τ_2: lifetime of the electrons in the photoanodes.

nanocrystallites means that the electrons undergo efficient transportation along the conducting network by TiO_2 nanocrystallites. The highest lifetime of 1212.8 μs is recorded from the DSSC with a $CoNi_{0.25}$ CE, which suggests that the impressive electrocatalytic activity has an accelerating effect for dye excitation, electron generation, and therefore electron flow from the excited dye to the conduction band of the TiO_2. This deduction could be confirmed by the dark *J–V* characteristics in Figure 3b, in which the peak current density follows the order $CoNi_{0.25} < CoNi_{0.33} < CoNi_{0.50} < CoNi_{0.20} < CoNi < Co < Ni$. The dark current in a DSSC device is attributed to the recombination of I_3^- with electrons in the conduction band of TiO_2. The smallest dark current for a $CoNi_{0.25}$-based DSSC indicates that the recombination of the I_3^- species on the TiO_2/electrolyte interface is retarded and the electron transportation along conducting channels is more efficient.

CEs are crucial components in solar panels applied as engines for vehicles. The requirements for a robust solar panel are fast start-up, multiple start/stop cycling, and stable photocurrent. Figure 5c shows the start-stop switches of the cell devices with $CoNi_{0.25}$ and Pt electrodes. An abrupt increase in the photocurrent density at "light on" means a fast start-up, whereas no delay in starting the cell demonstrates the high catalytic activity of the $CoNi_{0.25}$ alloy electrode for I_3^- reduction. The higher photocurrent density shows the superior catalysis of the $CoNi_{0.25}$ alloy compared to the Pt electrode. The photocurrent after seven start/stop cycles is the same as its initial state, which is a requirement for durable solar engines. To study the stability of the $CoNi_{0.25}$ alloy electrode under prolonged irradiation, the photocurrent density of the assembled DSSC was recorded with irradiation over 4 h. No sign of degradation can be detected 4 h (Figure 5d). The photocurrent densities decrease by 1.3% and 25.2% for the cells with $CoNi_{0.25}$ and Pt electrodes, respectively. Although the DSSC ist tested for only 4 h, this preliminary result demonstrates that the stability of a cell device can be improved by employing a $CoNi_{0.25}$ alloy electrode.

In summary, binary Co-Ni alloys with an fcc cubic structure have been fabricated by a mild hydrothermal reduction strategy free of any surfactant or template and employed as CE materials in DSSCs. It is demonstrated that the $CoNi_{0.25}$ alloy CE has an optimal charge-transfer ability and electrocatalytic activity toward I_3^- reduction. As a result of the elevated reaction kinetics with the $CoNi_{0.25}$ alloy, the photogenerated electrons can easily flow to the conduction band of TiO_2 with less recombination with I_3^- species. The DSSC with a $CoNi_{0.25}$ alloy CE exhibits an impressive power conversion efficiency of 8.39% in comparison to 6.96% for a device based on a pure Pt CE. The research presented here is far from being optimized, but these profound advantages along with low cost, mild synthesis, and scalable materials promise the Pt-free binary Co-Ni alloy CEs to be strong candidates in robust DSSCs. Further studies are now in progress to extend this approach to other Co-Ni alloy CEs with polymorphs.

Received: July 7, 2014
Published online: August 21, 2014

Keywords: alloys · counter electrodes · dye-sensitized solar cells · electrochemistry · energy conversion

[1] B. O'Regan, M. Grätzel, *Nature* **1991**, *353*, 737 – 740.
[2] U. Bach, T. Daeneke, *Angew. Chem.* **2012**, *124*, 10601 – 10603; *Angew. Chem. Int. Ed.* **2012**, *51*, 10451 – 10452.
[3] D. Kim, A. Ghicov, S. P. Albu, P. Schmuki, *J. Am. Chem. Soc.* **2008**, *130*, 16454 – 16455.
[4] G. R. Li, F. Wang, Q. W. Jiang, X. P. Gao, P. W. Shen, *Angew. Chem.* **2010**, *122*, 3735 – 3738; *Angew. Chem. Int. Ed.* **2010**, *49*, 3653 – 3656.
[5] Q. Tai, B. Chen, F. Guo, S. Xu, H. Hu, B. Sebo, X. Z. Zhao, *ACS Nano* **2011**, *5*, 3795 – 3799.
[6] Q. W. Tang, H. Y. Cai, S. S. Yuan, X. Wang, *J. Mater. Chem. A* **2013**, *1*, 317 – 323.
[7] L. Chen, J. P. Jin, X. Shu, J. B. Xia, *J. Power Sources* **2014**, *248*, 1234 – 1240.
[8] Q. H. Li, J. H. Wu, Q. W. Tang, Z. Lan, P. J. Li, J. M. Lin, L. Q. Fan, *Electrochem. Commun.* **2008**, *10*, 1299 – 1302.
[9] J. H. Wu, Q. H. Li, L. Q. Fan, Z. Lan, P. J. Li, J. M. Lin, S. C. Hao, *J. Power Sources* **2008**, *181*, 172 – 176.
[10] F. Gong, H. Wang, X. Xu, G. Zhou, Z. S. Wang, *J. Am. Chem. Soc.* **2012**, *134*, 10953 – 10958.
[11] D. Chen, H. Zhang, Y. Liu, J. H. Li, *Energy Environ. Sci.* **2013**, *6*, 1362 – 1387.
[12] X. Y. Cheng, Z. J. Zhou, Z. L. Hou, W. H. Zhou, S. X. Wu, *Sci. Adv. Mater.* **2013**, *5*, 1193 – 1198.
[13] Q. Xu, F. Liu, Y. Liu, K. Cui, X. Feng, W. Zhang, Y. Huang, *Sci. Rep.* **2013**, *3*, 2112.
[14] B. L. He, X. Meng, Q. W. Tang, *ACS Appl. Mater. Interfaces* **2014**, *6*, 4812 – 4818.
[15] B. L. He, X. Meng, Q. W. Tang, P. J. Li, S. S. Yuan, P. Z. Yang, *J. Power Sources* **2014**, *260*, 180 – 185.
[16] H. Y. Cai, Q. W. Tang, B. L. He, P. J. Li, *J. Power Sources* **2014**, *258*, 117 – 121.
[17] N. Li, C. W. Hu, M. H. Cao, *Phys. Chem. Chem. Phys.* **2013**, *15*, 7685 – 7689.
[18] L. Lin, Y. Chai, Y. Yang, X. Wang, D. He, Q. W. Tang, S. Ghoshroy, *Int. J. Hydrogen Energy* **2013**, *38*, 2634 – 2640.
[19] D. Kim, R. Shanmugam, M. R. Choi, B. Yoo, *Electrochim. Acta* **2012**, *75*, 42 – 48.
[20] C. Xu, J. Hou, X. Pang, X. Li, M. Zhu, B. Tang, *Int. J. Hydrogen Energy* **2012**, *37*, 10489 – 10498.
[21] G. J. Wang, Y. Z. Gao, Z. B. Wang, C. Y. Du, J. J. Wang, G. P. Yin, *J. Power Sources* **2010**, *195*, 185 – 189.
[22] B. L. He, Q. W. Tang, J. H. Luo, Q. H. Li, X. X. Chen, H. Y. Cai, *J. Power Sources* **2014**, *256*, 170 – 177.

[23] R. Bajpai, S. Roy, P. Kumar, P. Bajpai, N. Kulshrestha, J. Rafiee, N. Koratkar, D. S. Misra, *ACS Appl. Mater. Interfaces* **2011**, *3*, 3884 – 3889.
[24] M. Wu, X. Lin, Y. Wang, L. Wang, W. Guo, D. Qi, X. Peng, A. Hagfeldt, M. Grätzel, T. L. Ma, *J. Am. Chem. Soc.* **2012**, *134*, 3419 – 3428.
[25] M. K. Wang, A. M. Anghel, B. Marsan, N. C. Ha, N. Pootrakulchote, S. M. Zakeeruddin, M. Grätzel, *J. Am. Chem. Soc.* **2009**, *131*, 15976 – 15977.
[26] T. Daeneke, A. J. Mozer, T. H. Kwon, N. W. Duffy, A. B. Holmes, U. Bach, L. Spiccia, *Energy Environ. Sci.* **2012**, *5*, 7090 – 7099.
[27] J. Yoon, M. Jin, M. Lee, *Adv. Mater.* **2011**, *23*, 3974 – 3978.

